ARTICLE   OPEN

Check for updates

High-throughput analysis of Fröhlich-type polaron models

Pedro Miguel M. C. de Melo [1,2 ✉], Joao C. de Abreu [2], Bogdan Guster [3], Matteo Giantomassi [3], Zeila Zanolli [1], Xavier Gonze [3] and Matthieu J. Verstraete[2]

The electron–phonon interaction is central to condensed matter, e.g. through electrical resistance, superconductivity or the formation of polarons, and has a strong impact on observables such as band gaps or optical spectra. The most common framework for band energy corrections is the Fröhlich model, which often agrees qualitatively with experiments in polar materials, but has limits for complex cases. A generalized version includes anisotropic and degenerate electron bands, and multiple phonons. In this work, we identify trends and outliers for the Fröhlich models on 1260 materials. We test the limits of the Fröhlich models and their perturbative treatment, in particular the large polaron hypothesis. Among our extended dataset most materials host perturbative large polarons, but there are many instances that are non-perturbative and/or localize on distances of a few bond lengths. We find a variety of behaviors, and analyze extreme cases with huge zero-point renormalization using the first-principles Allen-Heine-Cardona approach.

INTRODUCTION

The correct assessment of the electronic band gap and properties of charge carriers is of primary importance in determining the utility and applicability of semiconductors and insulators. Theoretical treatments usually only include the "frozen-ion" electronic aspect of the problem. Over the past two decades it has become clear that this is a severe limitation given the accuracy of both measurements and more advanced theories[1–9].

The most common band-gap calculations involve Kohn-Sham Density Functional Theory (KS-DFT)[10–12] or the GW approximation from Many-body Perturbation Theory (MBPT), including different degrees of accuracy in the interactions between electrons[13,14]. MBPT computations are more computationally demanding than KS-DFT, but can yield band-gap results that are within 2% to 10% of experimental measurements[2]. However, both are zero-temperature formalisms: a crucial and often ignored effect is the electron–phonon interaction (EPI), which leads to a renormalization of the band gap as a function of temperature. Even at $T = 0$ K, EPI yields the so called zero-point renormalization of the band gap (ZPR_{c+v}), which combines conduction and valence band renormalizations (ZPR_c and ZPR_v).

Several theoretical approaches are available to calculate the ZPR_{c+v}, among which the Fröhlich model[15] and the perturbative approach proposed hy Allen, Heine and Cardona (AHC)[16–18]. In its first-principles version, AHC is the current gold standard for obtaining the ZPR_{c+v}[3,4,6,7,9,19–24], although its computational load is quite large. In order for the AHC approach to be valid, the EPI should not be too strong, since it relies on a perturbative treatment.

In the original Fröhlich model, the charge carrier dynamics is described by a one-band isotropic and parabolic dispersion, and couples to one dispersionless longitudinal optical phonon mode. The EPI is accounted for in a rather coarse fashion with a fixed analytic functional form, thanks to the hypothesis that the electron–phonon interaction is dominated by the long-range behavior of the Coulomb interaction, in effect washing out all

atomic details. Studies of this model have been numerous[25–28], and, depending on the EPI strength, can be done by perturbative means (weak coupling limit) or by a self-consistent approach to electron self-trapping by the phonon field (strong coupling limit). Some well-established techniques allow to cover the entire coupling strength range[26,27], but are either difficult to generalize to first-principles approaches or require enormous computational resources.

Very recently, a unified approach to polarons and phonon-induced band structure renormalization has been proposed, covering the whole coupling strength range[29,30]. It has been applied in both Fröhlich model and first-principles contexts.

Usually, the Fröhlich model is only considered for so-called "large" polarons, for which the atomic details are ignored, while the denomination "small polarons" corresponds to the case where the localization of the electronic wavefunction is comparable to interatomic distances, and self-trapping ubiquitous. As mentioned above, large polarons can be self-trapped as well, but in this case the self-trapping region is much larger than the interatomic distance.

More recently Miglio et al.[9] derived a generalized Fröhlich model (gFr), capturing a more realistic physical picture than the standard Fröhlich model (sFr), in which one accounts for anisotropic and/or degenerate electronic dispersion, coupled to multiple phonons modes, possibly anisotropic, but still preserving the intrinsic continuum hypothesis (i.e. long-wavelength limit).

While for the Fröhlich model and its generalization only the zone-center phonons are needed, the AHC formalism requires the full phonon spectrum over the whole Brillouin Zone (BZ), and involves the explicit calculation of EPI matrix elements, making it computationally much more costly. ZPR_{c+v} determined via the generalized Fröhlich model have shown comparable results to the AHC formalism for a set of materials that include oxides and II-VI compounds. However, for less ionic materials, its predictions are not on a par with AHC[9].

[1]Chemistry Department, Debye Institute for Nanomaterials Science and European Theoretical Spectroscopy Facility, Condensed Matter and Interfaces, Utrecht University, PO Box 80.000, 3508 TA Utrecht, The Netherlands. [2]Nanomat/Q-MAT/CESAM and European Theoretical Spectroscopy Facility, Université de Liège, B-4000 Liège, Belgium. [3]UCLouvain, Institute of Condensed Matter and Nanosciences (IMCN), Chemin des Étoiles 8, B-1348 Louvain-la-Neuve, Belgium. ✉email: p.m.monteirocamposdemelo@uu.nl

The materials studied in this work will be primarily polar, thus the use of the (generalized) Fröhlich model is natural for two reasons: they are expected to yield polarons, and the model is a much less computationally costly estimation of the ZPR_{c+v}. Given the recent developments on the Fröhlich model[9] and the prevalence of polarons in different classes of insulating materials[31], a thorough evaluation of the standard and generalized Fröhlich models over a broad range of materials is essential in order to establish validity and limiting behaviors of each model. One intrinsic aspect to the Fröhlich model is the continuum limit, i.e. ignoring the crystal details while assuming that the polaron wavefunction is much larger than the shortest distance between atoms: the assumption is that one deals with large polarons. Other models are more suitable to include some level of atomistic detail, such as the Holstein model[32,33], which is not discussed here. Independently of the length-scale aspect of the polaron problem, a qualitative criterion arises in the original Fröhlich model with coupling strength α. In a weak-coupling perturbative treatment of this model, at $\alpha \approx 6$ a breakdown occurs with the divergence of the effective mass. This is to say that beyond this point simple perturbation theories fail, and the polaron experiences an intermediate or strong coupling with the crystal lattice deformations. Below this qualitative limit, in the weak coupling limit ($\alpha < 6$), the straight perturbative approach to the Fröhlich model is in reasonably good agreement with more refined approaches such as Feynman's path integral variational approach[26] or diagrammatic Monte Carlo[27]. If the Fröhlich model for a given material points to a breakdown of the perturbative approach, it is likely that its AHC treatment is also bound to be unrealistic, since it is based on a similar perturbative hypothesis.

The overall goal of this work is to exploit existing datasets from the literature to evaluate the breadth of applicability of the Fröhlich model(s), be it(them) limited by the continuum limit or by the breakdown of perturbation theory. The latter has also a bearing on the applicability of the AHC treatment.

The development of high throughput workflows and database Application Programming Interfaces allows for fast queries of available information, allowing one to perform quick higher-level calculations and even train machine learning algorithms. In this work, we rely on the database from ref. [34], which provides the electronic band structure, geometry, dielectric tensors, and phonon properties (e.g. mode frequencies and eigendisplacements) for a set of 1521 insulating materials. These are selected according to the following criteria: from two to five chemical elements per unit cell; experimentally stable 3D structures; non-magnetic; insulating materials with a minimal DFT band gap. The missing data on band masses is computed via a high throughput computational flow employing both AbiPy and ABINIT as described in Sec. III D. In the end, 1260 materials have all needed quantities to parameterize a Fröhlich model Hamiltonian. The remaining 261 materials either have unstable phonon modes or their band extrema are not located along high-symmetry lines in the BZ, making automating the computation of the effective masses extremely difficult. We do not believe that their inclusion in this work would significantly alter the results shown herein.

We focus on indicators that could mark the potential of a material as a system with large or small polarons. These may be desirable (for optical properties) or undesirable (for transport) in different applications: more is not necessarily better. The essential quantities in the standard Fröhlich model α, and the parameters of its generalized form[9], are the dielectric tensor, the effective masses at the band extrema, the Born effective charge tensor, and the phonon frequencies, all of which are stored in the databases mentioned above.

The paper is structured as follows: We present the high-throughput results for the 1260 studied materials in Sec. II. We follow with Sec. II C by performing an *abinitio* validation using the AHC approach for selected materials, and we discuss outliers found using the Fröhlich model, such as materials with large ZPR and small coupling α, as well as materials with large ZPR and large α. In these cases the Fröhlich model should be treated in the strong-coupling limit, and the long-wavelength limit may fail entirely (these are two distinct cases). In Sec. III A we recap the theoretical background for the original Fröhlich model in describing large polarons, while in Sec. III B we summarize the recent developments of the generalized Fröhlich model.

RESULTS AND DISCUSSION

Standard Fröhlich model

As stated in Section I, we have 1260 insulators for which all necessary quantities are present to compute the ZPR^{sFr} and α using Eqs. (3) and (9). In Fig. 1 we show the dispersion map of these quantities for both valence and conduction band edges (positive and negative values of the ZPR, respectively). The color of each point indicates the presence of an element of a given group of the periodic table (as shown in the inset), according to the following order of precedence: blue for materials with an element from group 17 (halogens); if no halogen is present, orange for materials with elements from group 16 (chalcogenides); green for materials with an element from group 15 (pnictogens). If no element of any of these groups is present, the circle is brown.

Values of α for conduction states are almost entirely concentrated in the $\alpha < 5$ region, while valence values extend further into the $5 < \alpha < 15$ range. Plots of α correlation with the dielectric constants, effective mass, and phonon frequency are shown in Supplementary Fig. 9. The c/v difference comes from the distributions of bare effective masses for conduction and valence band edges[35] (shown in the top panel of Fig. 2), since ϵ^*_{sFr} and ω^{sFr}_{eff} are the same for a given material. The bulk of the ZPR distribution
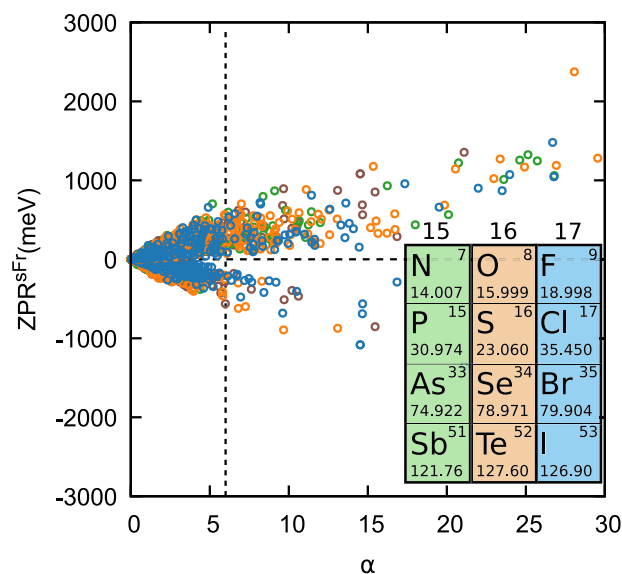

Fig. 1 Conduction (negative) and valence (positive) standard Fröhlich model ZPR^{sFr} and α values, for all but 10 (0) materials where the valence (conduction) ZPR^{sFr} exceeds 3000 meV. The ZPR^{sFr} values are determined based on the full range coupling strength described in Eq. (46). The color corresponds to chemical elements from groups 15 to 17 of the periodic table (see inset), and brown for all other compounds. Materials with compounds from group 17 are more concentrated in the $\alpha < 5$ domain, while materials with compounds from groups 16 and 14 have wider spreads. All classes of compound show outliers with very large α. Valence values are distributed over a wider range of α, and conduction values are more concentrated below $\alpha = 5$. The vertical dashed line is at $\alpha = 6$. An equivalent figure based on the full range α based on Feynman's approach is provided in Supplementary Fig. 8.
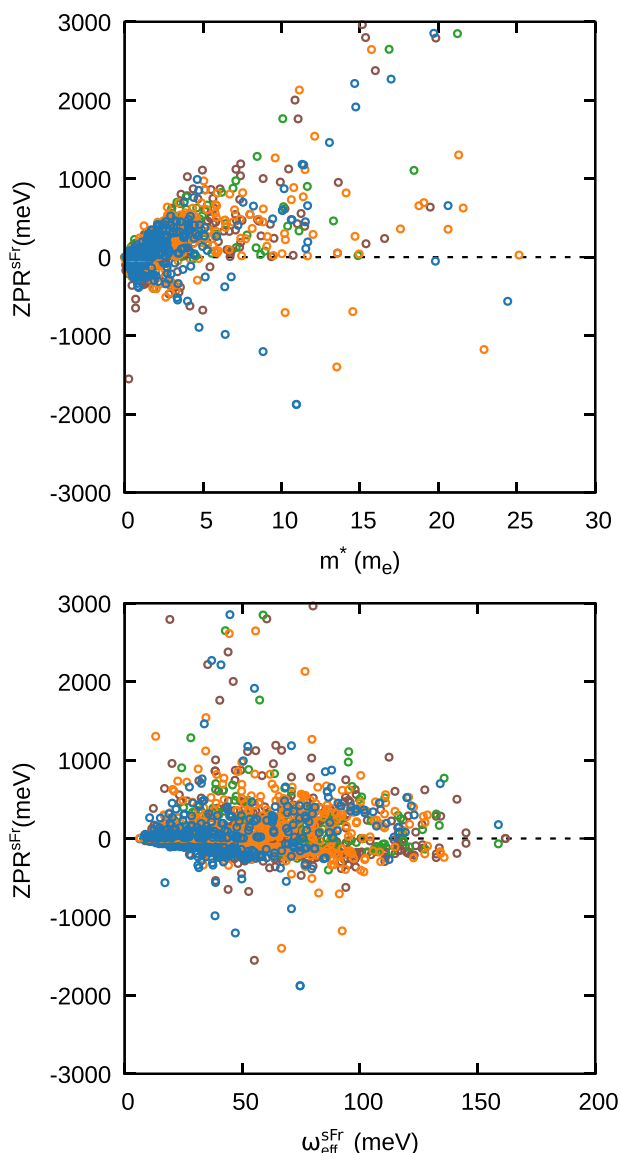
Fig. 2 Dispersion of conduction (negative) and valence (positive) ZPR^{sFr} energies versus the effective mass, m^*_{sFr} (top), and effective phonon frequency, ω^{sFr}_{eff} (bottom) for all materials with ZPR^{sFr} below 3000 meV. Same conventions as in Fig. 1. A rough square root behavior (Equation (10)) governs the maximum accessible ZPR^{sFr} for a given mass, and a degree of clustering is visible of the frequencies as a function of chemical period, with the lowest frequencies for halides, followed by chalcogenides, then the remaining materials. Dependence with the band effective mass (Eq. (32)) shows a dominant linear behavior, with a wider dispersion for valence bands when compared to the conduction band masses.

is within −500 meV (for conduction) and +1000 meV (for valence states). Parabolicity and isotropy of the considered electronic bands are fundamental hypotheses of the standard Fröhlich model. These hypotheses are broken by electronic structures presenting large effective masses ($m^* > 10$) in at least one direction. Huge ZPR values (i.e. >3 eV) can be observed in such cases.

The broad linear trend of the ZPR with respect to α in a family is visible for both conduction and valence bands, reflecting the simple proportionality through the ω^{sFr}_{eff} frequency in the lowest order of perturbation theory. Not all chemical families show the

same slope, even if the group of constituting element is taken into account, because the nuclear mass and bonding vary within a group and can strongly influence ω^{sFr}_{eff} and ϵ^0_{sFr}.

By looking at Eqs. (4), (46), and (47), we split the descriptors into two categories: the electronic properties $1/\epsilon^\infty_{sFr}$ and m^*_{sFr}; and the vibrational properties $1/\epsilon^*_{sFr}$ and ω^{sFr}_{eff}. Of these, only m^*_{sFr} and ω^{sFr}_{eff} show clear clustering or trends, see Fig. 2 for the effective mass and phonon frequency. The data shown in these figures allows one to further understand the dispersion of values shown in Fig. 1. The dielectric constants can be found in the Supplementary Fig. 8 which have very similar behavior as in Supplementary Figs. 6 and 7 given by Eq. (7). The highest values of m^*_{sFr} and $1/\epsilon^\infty_{sFr}$ are obtained in halides and chalcogenides, specifically in the conduction band. High effective mass (flat bands), with the same proportionality as the effective phonon frequency, are central to the larger ZPR. The largest conduction band effective masses come from transition metal halides with an empty d-band CBM, isolated due to crystal field splitting, which can become extremely flat (e.g. $CaTiF_6$). Large ω^{sFr}_{eff} does not mean high ZPR, as it can be seen in Fig. 2, even if the ZPR is proportional to $\sqrt{\omega^{sFr}_{eff}}$: other quantities are cross-correlated with ω^{sFr}_{eff}. Materials with one or more halogens are concentrated at the lower end of the distribution in phonon frequencies, but this is compensated by the other (electronic) parameters which can lead to both large α and ZPR^{sFr}. The conduction bands of these materials do not possess such heavy masses, and so the ZPR^{sFr} ends up being smaller.

A number of materials are beyond the $\alpha \leq 6$ limit of validity of perturbation theory for the standard Fröhlich model, suggesting the possible breakdown of the first-principles AHC approach as well.

In addition to the analysis of the validity of perturbation theory thanks to limits on α, the validity of the large polaron hypothesis can also be assessed. This hypothesis is crucial for the Fröhlich approach, be it in the standard form or in the generalized form. For this purpose, the polaron radius, Eq. (14), is computed, in the strong-coupling approximation. This is combined with the α data for both conduction and valence band edges in Fig. 3. Histogram distributions of α and a_P values are shown. An indicative value of $a_P = 10$ Bohr has been chosen to draw the frontier between small polarons and large polarons. Similarly, and as already discussed, values of α larger than 6 loosely indicate the breakdown of perturbation theory. Materials with small a_P will not be well reproduced with the long-range, large-polaron Fröhlich approximation. See Supplementary Table VI for the statistics of both electron and hole polarons. The number of cases yielding large polarons that can be described by perturbation theory is quite high: about 95% of the materials for electron and 65% for hole polarons. The large polaron hypothesis breaks down for about 5% of cases for electrons, and 35% of the hole polarons. The population of the top right quadrant of the two center plots in Fig. 3, namely materials for which the large polaron hypothesis is valid, but for which perturbation theory breaks down, is very small, below 1% both for electrons and holes. The opposite, bottom left quadrant, is more common, with smaller polarons in materials with modest $\alpha < 6$. Here the Fröhlich model should not apply at all, and the distinction for applying perturbation theory will be different depending on the approach used to treat the small/medium sized polaron.

The EPI enhancement of the bare electronic effective mass is shown in Fig. 4 and the distribution over the effective mass in Supplementary Fig. 5. The enhancement is determined based on the diagrammatic quantum Monte Carlo calculation proposed by Mishchenko et al. (see Fig. 5 in ref. [27]). Considering the improved generalized Fröhlich model, polaron anisotropy will shift many materials to lower critical radii, and the breakdown of perturbation theory can occur at lower α, as shown in ref. [36], where a similar
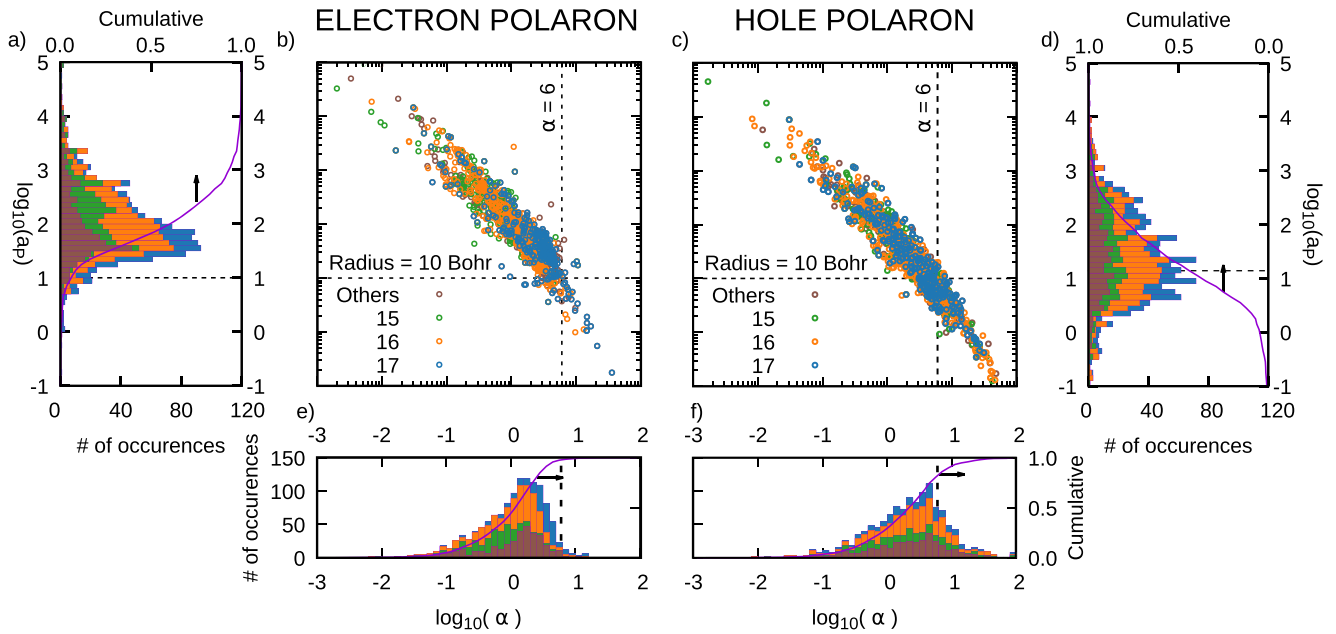
Fig. 3 Polaron radii and α distributions for both holes -c- and electrons -b- within the standard Fröhlich model. Dashed lines are indicative of the limits of Fröhlich perturbation theory ($α = 6$, perturbation theory breaking for larger values) and small polarons (indicatively $a_P = 10$ Bohr). Hole polarons are clearly heavier and more localized, but the majority of both distributions are within the limits of validity of the Fröhlich model and perturbation theory (upper left quadrants in **b** and **c**). Histograms -**a**, **d**, **e**, **f**- show the statistical and cumulative distributions, with stacked bar graphs for the different chemical periods. See Supplementary Table V for the distribution of radii and coupling strengths of both electron and hole polarons. Same color code as in Fig. 1.
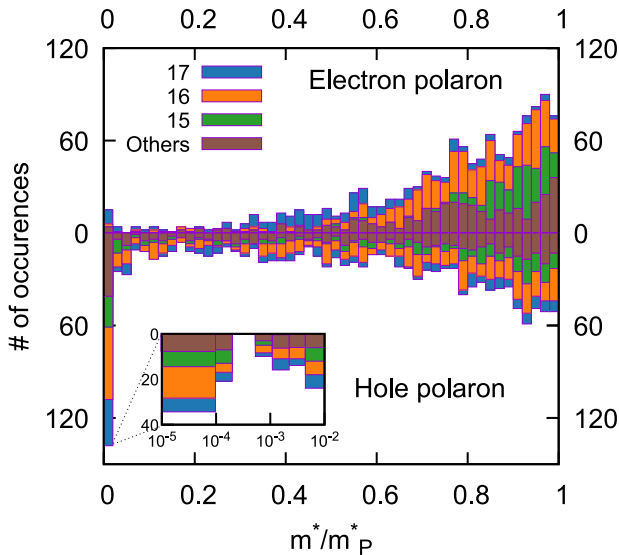

Fig. 4 Number of occurences of inverse effective mass enhancement, for both hole (upper part) and electron (lower part) polarons within the standard Fröhlich model. Stacked bars correspond to chemical period. On the right, the ratio between polaron mass and bare mass is close to one, while on the left, the polaron mass is much larger (in absolute value). The inset shows the distribution for very heavy hole polarons with huge mass enhancement. The effective mass enhancement is based on the mapping provided by the Diagrammatic Monte Carlo results (see Fig. 5 in ref. [27]) and Eq. (12). Same color code as in Fig. 1.

analysis of the distribution of $α$ and a_P was performed for a much smaller set of materials, all exhibiting cubic symmetry.

On this basis, the large polaron hypothesis with perturbative treatment might still be appropriate to treat the electron polaron for a majority of materials, but this might not be true to treat the valence band. The breakdown of perturbation

theory for $α > 6$, implying also that first-principles AHC theory would be inappropriate, is less often encountered, even for valence bands.

Generalized Fröhlich model

We now compare our results to the generalized Fröhlich model discussed in Section III B. Here we define the direction-dependent dielectric tensor as $\epsilon^∞(\hat{q}) = \sum_{αβ} \hat{q}_α \epsilon^∞_{αβ} \hat{q}_β$, and take into account all phonon modes with their respective direction dependence $ω^*_{j0}(\hat{q})$ and coupling, $\epsilon^*_j(\hat{q})$, and the direction-dependent effective mass inside Eq. (17). To evaluate the directional dependence, all quantities that depend on $\hat{q}$ are computed on a sphere of radius 10^{-4} Bohr^{-1}, using a total of 2000 points to sample the sphere. The phonon frequencies and eigendisplacements are interpolated on this grid using the *anaddb* tool in the ABINIT software package. Note that all parameters (e.g. k-point grids, energy cutoffs, pseudo potentials) are the same for the evaluation of all quantities involved. Differences that arise will come only from the nature of each method, namely that in the generalized model the angular dependency of all quantities is taken into account and the effects of all phonon modes are included, weighted by the mode-polarity vectors.

For the generalized Fröhlich model, no all-range calculations of the Feynman or DMC type have been performed until now. We have thus to rely on the perturbative result, Eq. (25), to obtain the ZPR. Coherently, the lowest order of perturbation, Eq. (10), is used to compare with the standard Fröhlich model.

In Fig. 5 we show the comparison between the effective (i.e. Hellwarth-modified) standard and the generalized Fröhlich model ZPR, both obtained in low-order perturbation theory, that we denote ZPR^{sFr} and ZPR^{gFr}, respectively, and $α$, that we denote $α^{sFr}$ and $α^{gFr}$, respectively. While it is not apparent to the naked eye, ZPR values for binary cubic systems match in both the generalized and standard models (see the file binarycubicZPRcomparison.json provided as SI). From Fig. 5 it is apparent that the standard and generalized models give very close results for the ZPR energy. This
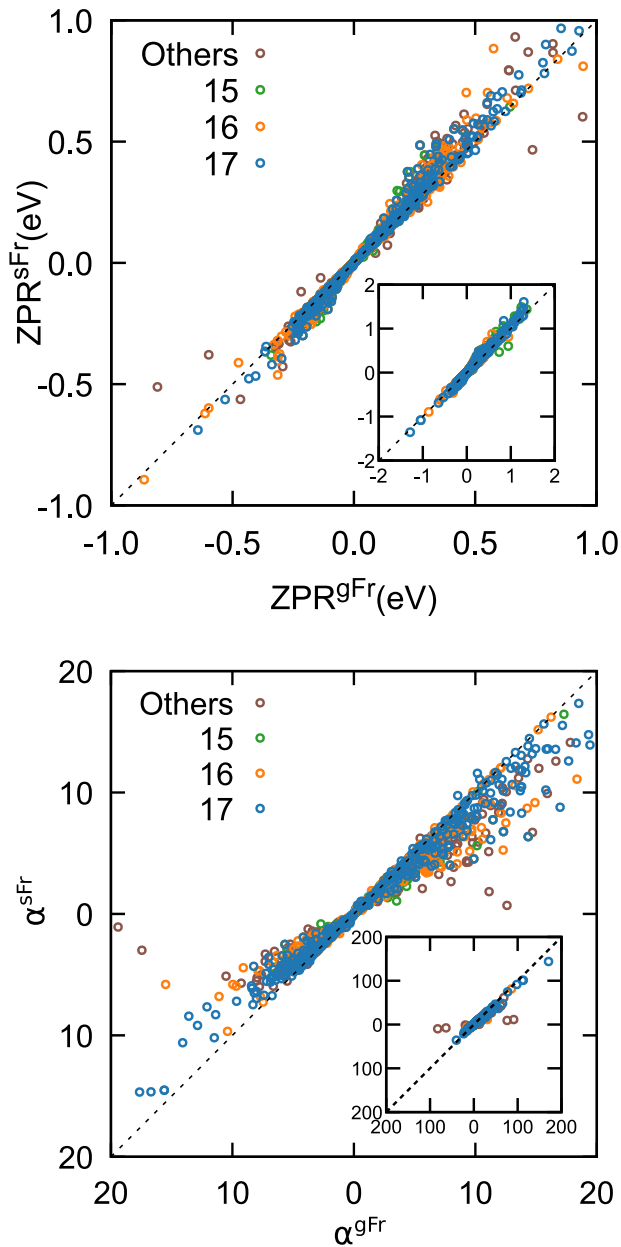
Fig. 5 Comparison of generalized and standard Fröhlich model for ZPR (top) and α (bottom), from perturbation theory, for both valence and conduction band edges. The insets show the dispersion for the full range of values of ZPR and α. The standard ZPR is usually slightly larger than the generalized Fröhlich model (at most by a factor of 2), and the $α^{sFr}$ is slightly smaller than $α^{gFr}$, with a wider spread (up to a factor of 3 or more) and fewer exceptions where $α^{gFr} < α^{sFr}$. This shows that different factors influence the ZPR and α, in particular the frequency which switches between the numerator and denominator.

is a surprising result, given the simplicity of the expressions used in the standard model, especially when one considers that there are no explicit phonon frequencies involved in Eqs. (44) and (45) (the LO frequencies are reconstructed from the Z^* and the $ε$). Nevertheless, the improvements brought by (1) a correct accounting for the anisotropy of $ε^*$ and $m^*(\hat{q})$, and (2) the inclusion of the Born effective charges and the atomic masses, make the simpler method a good approximation when compared to the generalized version. The fact that all these averaging procedures are evaluated separately is less critical on average, and

explains some of the spread in Fig. 5. In Supplementary Fig. 10 we show a comparison of the ZPR between the two models as a function of the spread of the anisotropy of the effective masses.

Some outliers were identified in Fig. 1a, for which $|ZPR^{sFr}| < |ZPR^{gFr}|$. For both the valence and conduction corrections these materials are: K_3NO_3, $CsNO_2$, $RbNO_2$, $NaNO_2$. These four materials share a particular feature in their phonon dispersion: an extremely flat phonon mode at around 800 cm^{-1}, followed by dispersive high frequency modes close to 1200 cm^{-1}. The outliers point to an interesting feature of the standard model: since the $ω_{LO}$ mode is replaced by an effective frequency, the contributions from modes with very high frequencies are diluted in the sum. However, the generalized model is still sensitive to them, which then leads to higher corrections.

Other interesting outliers were found when scanning through the values of ZPR and α in both models for binary compounds, including a family of alkali metal nitrides with the chemical formula XN_3. These are discussed in the next sections, together with other materials which have large ZPR due to a high number of fluorine ions, comparing to benchmark results from a fully first-principles method.

Ab initio benchmarking

The generalized Fröhlich model is expected to be more physically accurate than the standard model. In order to benchmark both Fröhlich models, we compare them with fully ab initio (AHC) calculations of the ZPR. As the latter are much more costly, we have selected a limited set of representative and/or simple test cases. Like the generalized Fröhlich model, the first-principles AHC approach works in the lowest order of perturbation.

Previously, Miglio et al[9] computed ZPR from first-principles for a set of 30 materials and compared them with the generalized Fröhlich model. Most of the stronger ionic compounds (oxides and chalcogenides) were well described by the model, within 25% error compared to the first-principles AHC approach. For nitrides, the ZPR were less accurate but still within 50% error. Their ZPR was twice larger in first-principles calculations than using the generalized Fröhlich model. We calculate the valence band ZPR for an intersecting subset of 19 materials (Supplementary Table VII) based on the generalized ZPR for cubic materials, Eq. (31), to establish the validity of the treatment for cubic materials where electronic and lattice components can be essentially treated independently. Moreover, the "cubic" aspect of the treatment refers solely to the lattice component of the problem, which makes the solution available away from crystal cubic symmetry, if we can assume an isotropic dielectric tensor.

In addition, we have chosen specific systems with high ZPR from our high throughput Standard Fröhlich survey, combined with either low, medium, or high α. Despite our theories being based on a perturbative approach, the stronger coupling cases are nevertheless instructive as it is expected that the similarity or difference within a common perturbative framework of the same order will translate to a similarity or difference within more elaborate frameworks that are able to tackle non-perturbative behaviors. The first case of lower α are four ionic molecular crystal azides: KN_3 and RbN_3 crystallize in a tetragonal system, LiN_3 and NaN_3 in a monoclinic system; the following case contains the trigonal system $CsNO_2$ (medium α); and, for the final extreme case we examine cubic Cs_2NaScF_6, tetragonal Li_2CaHfF_8 and trigonal K_2TiF_6. Finally for very low α the Fröhlich model is not expected to function, as non-polar modes will probably intervene. We will discuss these below comparing to AHC.

The main parameters of the standard and generalized Fröhlich approaches are shown in Supplementary Tables I and II, respectively, for our benchmark materials. In Supplementary Table III we compare the two models and the non-adiabatic AHC calculated ZPRs, as also depicted in Fig. 6.
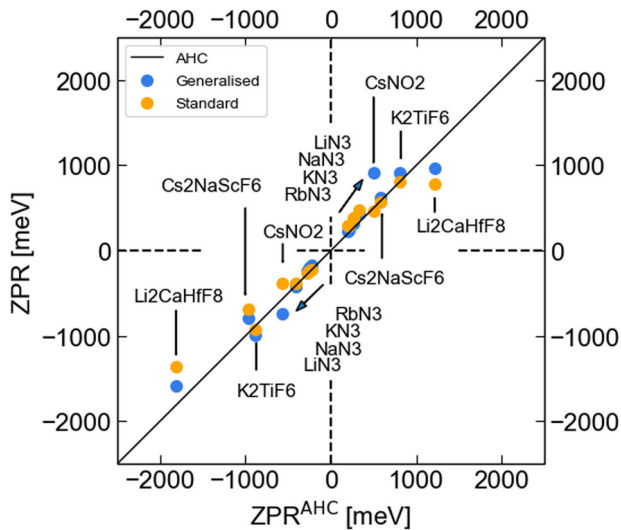
Fig. 6 Comparison of the ZPR for some chosen systems. The VBM (positive, right top part) and CBM (negative, left bottom part) ZPRs were calculated using the standard and generalized Fröhlich models and the non-adiabatic AHC approach.
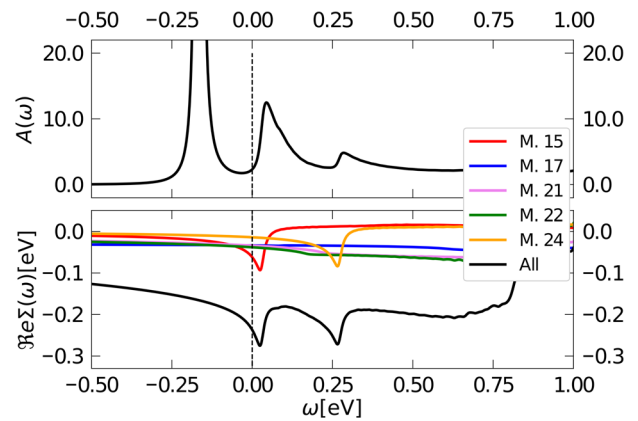

Fig. 7 Spectral function, $A(\omega)$ (top) and the real part of the self-energy, $\Re e\Sigma(\omega)$ (bottom) for KN$_3$ at the CBM. The self-energy is split by phonon mode for the largest contributions to the ZPR$_c$ as in Supplementary Table III. Only phonon modes 15 and 24 are LO, the others are non-LO.

In Fig. 6, we see that overall the standard Fröhlich model gives values similar to those of the generalized Fröhlich model, close to the non-adiabatic AHC ZPR at low α and dispersed for higher α. The methods rely on different averages over the LO-phonon modes. The former averages global quantities, for example, the Born effective charges, ionic masses, and the dielectric constants, while the latter accumulates the microscopic contribution to the ZPR over all directions as $\mathbf{q} \to 0$. One observes that some error cancellation occurs in the standard method giving sometimes "better" results than the generalized one.

There are still important contributions missing from these Fröhlich models, such as the non-polar and TO phonon modes, but the dominant qualitative physics is already present in both approaches. The difference between the modeled ZPRs and the non-adiabatic AHC, as shown in Supplementary Table III, does not allow us to draw any easy conclusion of which method is more accurate. On one side, the standard Fröhlich is simple to calculate, on the other side, the generalized Fröhlich model is physically more accurate and insightful.

From Supplementary Table II, we can retrieve four compounds with the highest discrepancy between the standard and the generalized Fröhlich models, the RbN$_3$ and CsNO$_2$ systems, followed by KN$_3$ and Li$_2$CaHfF$_8$. The first three compounds have a smaller sum of their inverse atomic masses with respect to the others (Supplementary Table I). The Li$_2$CaHfF$_8$ compound has the highest number of light atoms in the unit cell, in spite of this, it has one of the most dispersed Born effective charges of the selected systems, i.e., the polarizability and the atomic displacements are not aligned. The same dispersion appears in CsNO$_2$.

In the following Sections (II D for KN$_3$ and II E for Cs$_2$NaScF$_6$), we determine the features which produce differences between the standard and generalized Fröhlich approaches, and with the non-adiabatic AHC method.

Ab initio Azides: large ZPR, small α

Changes in the variables to calculate α and ZPR in the azides can be mainly interpreted by trends in the ionic radius (decrease) and in the electronegativity (increasing from Rb, K, Na, to Li)[37], leading to a decrease of the unit cell volume and the dielectric constant, and an increase of the effective mass.

The average of the ω_{LO} modes for both standard and generalized Fröhlich methods are similar in the RbN$_3$ and KN$_3$

systems but start to differ for the NaN$_3$ and LiN$_3$. For the generalized Fröhlich model, the frequencies decrease together with the atomic mass, as opposed to the standard model. Since there is a discrepancy between the averaged effective dielectric constants, the opposite change of the frequencies leads to an approximation between the generalized and standard ZPRs.

The calculations of the generalized Fröhlich ZPR relatively improves at the CBM as the atomic masses of the cations decrease and the opposite occurs for the VBM. Relative changes at the standard model are less consequential, however, it has relative high accuracy at the CBM and much less at the VBM.

In the standard Fröhlich model the value of α of KN$_3$ is smaller than, for example, the KF system. Even if both have a similar fraction $\sqrt{m^*}/e^*$ (0.29 for KF and 0.23 for KN$_3$) KN$_3$ has a higher range of phonon frequencies of 271 meV than KF (42 meV), leading to an $\omega_{\text{eff}}^{\text{sFr}}$ of 73 and 39 meV, respectively. The very high range of frequencies of KN$_3$ comes from the resonances created by the linear chains of N$_3$ harmonic oscillators, where all three atoms vibrate along the bonds. The same reasoning can be applied to the other azides.

In the case of KN$_3$ (with the electronic and phononic band structure and density of states shown in Supplementary Figures 1 and 2), there are two active LO phonon modes in the generalized Fröhlich approach (see bottom of Supplementary Table IV). The phonon mode with highest contribution (76%) to the ZPR is LO phonon mode j=15 with a frequency of 20 meV, and not the highest LO mode (j=24) with a frequency of 260 meV.

The averaging over $\hat{q}$ directions, overestimates the value of α compared to the standard Fröhlich model.

Going beyond the generalized Fröhlich approach and deconstructing the non-adiabatic AHC ZPR into its phonon mode components (see top of Supplementary Table IV and Supplementary Figure 4), we find that the highest contribution of 26.14% to the total ZPR comes from LO phonon mode 15 and that there are non-LO phonon modes (20, 21 and 22, excluded from the Fröhlich models) which have even higher contribution to the ZPR than the highest frequency LO phonon mode 24.

Several factors contribute to the spread of the ZPR contribution throughout the different phonon states. One key attribute is the polarizability and eigenvectors of the modes. Phonon mode 15 in KN$_3$ has a stronger polarizability than the highest phonon mode, which is mostly driven by the lightest atoms. Mode 15 has a mix of contributions between the potassium and nitrogen atomic vibrations, with larger dipoles, and hence a larger mode polarizability.
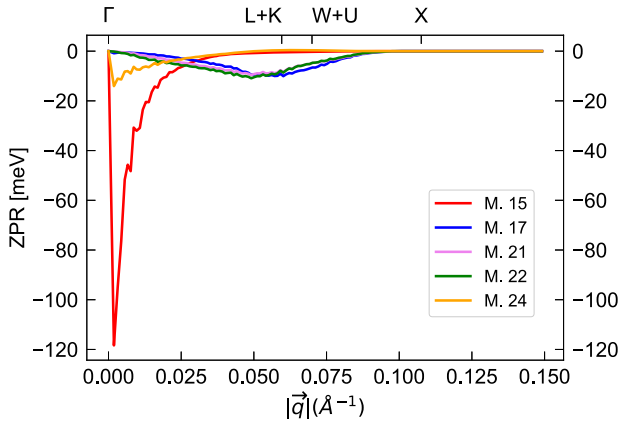
Fig. 8 Spherical accumulation of the ZPR$_c$ of KN$_3$ as a function of the norm of the vector |q| for each phonon mode. The calculations were done using the $64 \times 64 \times 64$ q-grid sampling. The norms of selected high symmetry points are shown on the top axis. The phonon modes 15 and 24 are LO polar mode, and all the others are non-LO phonon modes.

Fig. 9 Spectral function, A(ω) (top) and the real part of the self-energy, $\Re e\Sigma(\omega)$ (bottom) for Cs$_2$NaScF$_6$ at the CBM. The self-energy is split by phonon mode for the largest contributions to the ZPR$_c$ as in Supplementary Table IV. The frequency range is limited to the satellites: the two QP peaks at -0.249 and 0.341 eV are not visible in this range. The first peak in A(ω) comes from a mode with low contribution to the full ZPR, which is only a small bump in the total $\Re e\Sigma(\omega)$. The phonon modes 18, 24, and 30 are LO, and phonon mode 29 is non-LO.

A second key factor is the inclusion of non-LO modes. In Fig. 7, we show the electron self-energy of KN$_3$ (bottom) and the spectral function (top). The LO-phonons can be found in the self-energy with characteristic Fröhlich peaks[38]. Specifically in KN$_3$, the self-energy terms for phonon modes 15 and 24 show a peak at their Γ point phonon frequency (the KS energy is at 0.0 eV). Mode 17 is also LO, but the peak amplitude is small, around 1 meV. In addition to their contribution to the ZPR binding energy, the LO-phonon modes are also responsible for satellites in the spectral function visible in the top panel.

The non-LO phonon modes (either TO or non-polar) do not show peaks but a type of plateau starting at their Γ point phonon frequencies, linked to long-range quadrupole potential[39,40] and/or short-range fields[41]. At the KS energy, where the ZPR is evaluated, their $\Re e\Sigma(\varepsilon)$ is not negligible at all, with a net contribution larger than that of the LO modes.

Another way to distinguish contributions to the ZPR is by plotting their dependency on the phonon wavevector (norm), as in Fig. 8. The two LO phonon modes have their main contributions from wavevectors close to Γ, and correspond to long-range electric dipole fields. The non-LO phonon modes ($j = 17, 21$, and 22) originate at the boundary of the Brillouin zone, and correspond to interactions with shorter-range crystal fields. Note that it is important in this analysis to avoid mixing LO and non-LO band contributions when their frequencies cross away from Γ, by following the irreducible representations and character of each mode to attribute the ZPR(j, q) contributions.

Ab initio Cs$_2$NaScF$_6$: large ZPR, large alpha

The ZPR$_c$ of the Cs$_2$NaScF$_6$ compound is much higher than the azides with a value of -966.1 meV in the non-adiabatic AHC. In addition to the small increase of the effective dielectric constant contribution, there is also an approximately 8-fold increase of the effective mass compared with the azides (Supplementary Table I). The Cs$_2$NaScF$_6$ electron band structure and the projected density of states are shown in Supplementary Figure 3. The bottom conduction band has very low dispersion which translates into a large effective mass and localized electrons, which are found in the Sc-F bonds. The main source of the high ZPR is the coupling between the (high frequency) vibrations of F atoms and the d-orbital conduction band of Sc.

For Cs$_2$NaScF$_6$ the generalized and standard Fröhlich models are not as simply ranked: gFr is better for the VBM, while sFr is slightly
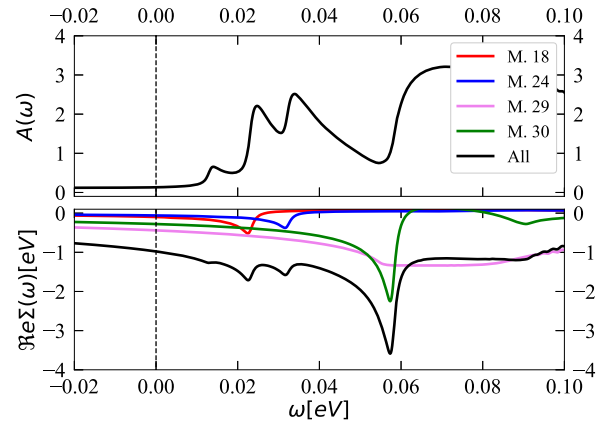
better for the CBM. The ZPR calculated within the generalized Fröhlich and non-adiabatic AHC can be split into phonon mode contributions (Supplementary Table V) with the phonon band structure shown in Supplementary Figure 4. Again unlike the case of the azides, the highest ZPR contribution is the non-LO phonon mode 29, contributing almost 45% and an α_i of 9.20. Generalized Fröhlich ignores the non-LO phonons, which, in this case, are close to the ω_{LO}. Part of this contribution is spread to lower LO phonon modes leading to a worse ZPR.

The real part of the self-energy for phonon mode 29 is the most important at the KS energy (0.0 in Fig. 9), and increases towards its Γ-point phonon frequency (47.8 meV) but it has no peak. The phonon mode with the highest frequency is a LO phonon mode, showing a green peak in the self-energy figure, but has a smaller contribution of around 28.5% to the total ZPR. The other phonon modes shown in the figure are also LO phonon modes and have small self-energy peaks at their Γ point phonon frequencies. The spectral function shape is complicated by the presence of two quasi particle solutions (not visible in the figure), which convolute the full self-energy. This is more common in the electron–phonon case (as opposed to electron-electron) as the self-energy amplitude is of the same order of magnitude as the phonon energies (or even larger).

The angle-integrated ZPR as a function of wavevector norm (Fig. 10) shows the Fröhlich-like behavior close to |q| = 0 for $j = 18$, 24, and 30. Mode 29 behaves as $|q|^2$ following the volume contribution $4\pi|q|^2$ in the angular average, which means the ZPR contributions are relatively constant throughout the Brillouin zone.

As a summary, for the set of materials considered in the section IIc, d, and e, we observe that the standard and generalized Fröhlich models are both close to the full first-principles bench-mark calculations. One characteristic of high-frequency range materials, as in the azides, is the geometrical isolation of the lighter atoms. The averaging of the LO frequencies are similar in both Fröhlich models for homogeneous and heavy unit cells and they differ for inhomogeneous and lighter unit cells. The directional averaging in phonon wavevector overestimates α when comparing to standard α that is dependent on tensors of the macroscopic quantities. There is no direct way to determine which method provides the closest results to non-adiabatic AHC
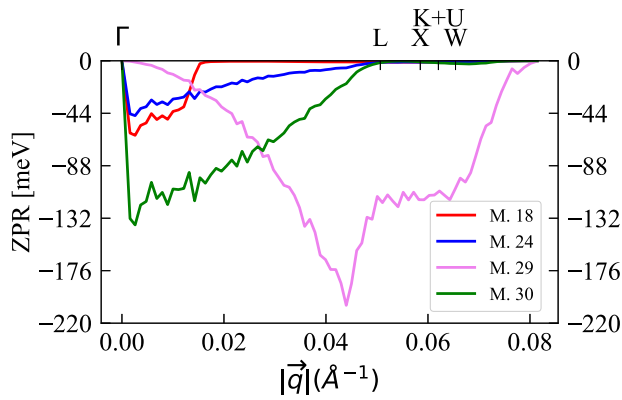
Fig. 10 Spherical accumulation of the ZPR_c of Cs_2NaScF_6 as a function of the norm of the vector |q| for each phonon mode. The calculations were done using the $64 \times 64 \times 64$**q**-grid sampling. The high-symmetry k-points K and U are between X and W. The phonon modes 18, 24, and 30 are LO polar modes, contrarily the mode 29 is non-LO phonon mode.

for an arbitrary compound, because there are some error cancellations in the standard Fröhlich method which can give better results than by explicitly treating all of the LO phonons through the generalized Fröhlich approach. In addition, ignoring non-LO modes can worsen both models, especially if the non-LO phonon mode is close to ω_{LO}, exaggerating the importance of lower frequencies and widening the distance from the non-adiabatic AHC ZPR. One must keep in mind that the AHC theory is not the final physical answer for very strong EPC, as small polarons will be formed, but it is a well-defined and rigorous reference point, and comparing to the Fröhlich model at large coupling it seems all of these theories may function even at much higher values of α.

Considering now the results in their globality, in our study, the polaron binding energy, or zero point renormalization, is evaluated in both standard and generalized Fröhlich models for a database of 1260 materials. Lowest order perturbation theory is used for the generalized Fröhlich model, while both perturbative and all-range formulas are available for the standard model, once the single parameter α is defined. In order to apply the standard Fröhlich expression to complex solids, a set of averaging procedures is proposed, for the effective phonon frequency, mass, and dielectric constant, expanding on a previous work[42] of Hellwarth and Baggio.

A broad range of validity is found for both models: 58% of valence bands and 91% of conduction band polarons are in the Fröhlich limit of weak coupling and large radius. Our effective standard and the generalized model ZPR are in good quantitative agreement with fully ab initio spot checks using the Allen-Heine-Cardona theory. The generalized Fröhlich model ZPR includes a fully coherent directional averaging of the dielectric, phononic, and electron band parameters, whereas the "effective standard" Fröhlich model averages each parameter. One finds distinctive trends depending on the material's composition: more electronegative compounds containing halogens or chalcogens generally present higher ZPR associated with higher α. Compounds containing group 13 elements show rather lower ZPR, though there are outliers in all categories.

Given the broad range of behaviors in our set of materials, we benchmark our studies with fully ab initio DFT-based non-adiabatic AHC calculations of the ZPR. We focus on outlier materials with different α (low, medium, and high) and high ZPR. Both Fröhlich models follow the ZPR trend of the non-adiabatic AHC quite closely. The residual difference between the Fröhlich models and the AHC results is a combination of important non-LO phonon modes, and the details of the mode and wavevector

distribution of the electron–phonon coupling. We wish to stress that predicting a ZPR close to the full AHC value makes the Fröhlich models useful, but does not mean that all of the physics is captured: we show that non-polar modes can even dominate the total ZPR.

The standard Fröhlich model can fail in more than one way: due to essential non-LO phonons modes, anisotropy, or the breakdown of perturbation theory. However, regardless of the Fröhlich method's limitations, strong evidence is provided for the ubiquity of Fröhlich-type large polaron formation, for the range of possible behaviors and parameter space, and the importance of polarons in providing reliable band gaps and effective masses. Interestingly, for a small number of weak coupling cases, the estimated polaron radius is small enough to call into question the applicability of Fröhlich models.

METHODS

The standard Fröhlich model

The Fröhlich model[15,43] assumes a system with a single parabolic electron band of effective isotropic mass m^* and a single non-dispersive longitudinal optical phonon branch of frequency ω_{LO}. The electron–phonon interaction comes from the macroscopically screened Coulomb interaction between electrons and the nuclei moving along the optical phonon mode. While the latter approximation is dominant and qualitatively correct for $\mathbf{q} \approx 0$, it is assumed to be valid in the whole Brillouin zone, which corresponds to a continuum treatment, in line with the hypotheses of an isotropic electronic band and non-dispersive phonons. This means that there are no Debye-Waller contributions to the electron–phonon interaction, and transverse optical or acoustic modes are ignored. This model also ignores band degeneracies and the possibility of different band masses and warping[44]. Although formulated initially for a conduction electron, it can be easily applied to valence electrons, with a proper change of sign in selected formulas.

For a material with non-degenerate isotropic band extrema and isotropic dielectric function, one can write the following Hamiltonian for the standard Fröhlich model[45] for an electron (in atomic units $\hbar = 1$, $a_{\text{Bohr}} = 1$, $m = 1$, and the Born and Huang convention for $\mathbf{q}$ and $-\mathbf{q}$ phonon eigenvectors is followed[46]):

$$\hat{H}^{sFr} = \sum_{\mathbf{k}} \frac{\mathbf{k}^2}{2m^*}\hat{c}_{\mathbf{k}}^{\dagger}\hat{c}_{\mathbf{k}} + \sum_{\mathbf{q}} \omega_{LO}\hat{a}_{\mathbf{q}}^{\dagger}\hat{a}_{\mathbf{q}} + \sum_{\mathbf{k},\mathbf{q}} g^{sFr}(\mathbf{q})\hat{c}_{\mathbf{k}+\mathbf{q}}^{\dagger}\hat{c}_{\mathbf{k}}\left(\hat{a}_{\mathbf{q}}^{\dagger} + \hat{a}_{-\mathbf{q}}\right), \quad (1)$$

where the electron–phonon coupling constant is given by

$$g^{sFr}(\mathbf{q}) = \frac{1}{q}\left(\frac{2\pi\omega_{LO}}{\epsilon^* V_{BvK}}\right)^{\frac{1}{2}} = \frac{1}{q}\left(\frac{2\sqrt{2}\pi}{V_{BvK}}\frac{\omega_{LO}^{3/2}}{\sqrt{m^*}}\alpha\right)^{\frac{1}{2}}, \quad (2)$$

V_{BvK} is the Born von Kármán supercell volume, the dimensionless coupling parameter α is

$$\alpha = \frac{1}{\epsilon^*}\sqrt{\frac{m^*}{2\omega_{LO}}}, \quad (3)$$

where ϵ^* is defined by

$$\frac{1}{\epsilon^*} = \frac{1}{\epsilon^{\infty}} - \frac{1}{\epsilon^0}. \quad (4)$$

As a side note, ϵ^*, ϵ^{∞} and ϵ^0 are independent of the nuclear masses: ϵ^{∞} is purely electronic, while ϵ^0 is obtained in the adiabatic limit (low-frequency limit), so that the nuclei have time to adjust adiabatically to the applied electric field, regardless of their mass. ϵ^* is always greater than ϵ^{∞}. For polar compounds with strong ionic screening, the difference in ϵ's will be large and $\epsilon^* \to \epsilon^{\infty}$, whereas for purely covalent compounds or mono-atomic compounds $\epsilon^0 \simeq \epsilon^{\infty}$, and so $\epsilon^* \to \infty$, which runs counter to intuition for habitual dielectric responses, but simply pushes α to 0 in the Fröhlich model.

The Hamiltonian in Eq. (1) can be simplified by using a different choice of units:

$$\hat{H}^{\text{sFr}} = \sum_{\mathbf{k}} \frac{\mathbf{k}^2}{2} \hat{c}_{\mathbf{k}}^{\dagger} \hat{c}_{\mathbf{k}} + \sum_{\mathbf{q}} \hat{a}_{\mathbf{q}}^{\dagger} \hat{a}_{\mathbf{q}} + \sum_{\mathbf{k},\mathbf{q}} \frac{1}{q} \left(\frac{2\sqrt{2}\pi\alpha}{V_{\text{BvK}}} \right)^{\frac{1}{2}} \hat{c}_{\mathbf{k}+\mathbf{q}}^{\dagger} \hat{c}_{\mathbf{k}} \left(\hat{a}_{\mathbf{q}}^{\dagger} + \hat{a}_{-\mathbf{q}} \right),$$

(5)

where the energies, momenta, and length were rescaled by factors of ω_{LO}, $(\omega_{\text{LO}} m^*)^{1/2}$, and $(\omega_{\text{LO}} m^*)^{-1/2}$, respectively. With this choice, it becomes clear that the sole free parameter α characterizes the strength of the electron–phonon interaction with respect to the intrinsic electron and phonon terms.

Perturbation theory can be used to treat the Hamiltonian Eq. (5) in the limit of small α, delivering the polaron binding energy (ZPR) (again in atomic units) as

$$E_{\text{P}} = -\omega_{\text{LO}}(\alpha + 0.0159\alpha^2 + ...).$$

(6)

A more accurate approach based on the Feynman path integral[26] can be employed, covering the whole range of coupling strengths, as follows:

$$E_{\text{P}} = -\omega_{\text{LO}}(\alpha + 0.98(\alpha/10)^2 + 0.60(\alpha/10)^3 \\ + 0.14(\alpha/10)^4), \text{ for } \alpha \leq 5;$$

(7)

$$E_{\text{P}} = -\omega_{\text{LO}}(0.106\alpha^2 + 2.83), \text{ for } \alpha \geq 5.$$

With the same perturbative treatment, it is possible to show that the ratio between the effective masses of the polaron, m_{P}^*, and the electron is approximately given by

$$\frac{m_{\text{P}}^*}{m^*} = \left(1 - \frac{\alpha}{6} + 0.00417\alpha^2 + ...\right)^{-1}.$$

(8)

At the lowest order of perturbation theory, one obtains the well-known formula

$$E_{\text{P}} \approx -\alpha\omega_{\text{LO}},$$

(9)

or more explicitly,

$$E_{\text{P}} = -\frac{1}{\epsilon^*} \sqrt{\frac{m^*\omega_{\text{LO}}}{2}},$$

(10)

where ω_{LO} contains the only dependence on nuclear masses. At this order in the expansion Eq. (8) yields the following polaron mass:

$$\frac{m_{\text{P}}^*}{m^*} \approx \left(1 - \frac{\alpha}{6}\right)^{-1},$$

(11)

with the immediate consequence that at $\alpha = 6$ the polaron mass diverges and this low-order perturbation theory approach is no longer valid. This parameter thus also provides a breakdown point for the lowest-order perturbative treatment of the Fröhlich model.

A large α is physically associated with the appearance of self-localization of the electron due to the phonon response, a non-perturbative phenomenon that can be treated, alternatively, in the so-called "strong-coupling" limit of the Fröhlich model. Thus the $\alpha = 6$ value suggests a change of regime for the Fröhlich polaron (nothing abrupt, though). Nevertheless, the occurrence of the wide range of behaviors present in our set of 1260 materials demands a more careful treatment in describing the polaron effective mass in the standard Fröhlich model: we make use of the results based on the Diagrammatic Monte Carlo method applied to the standard Fröhlich model[27], by mapping the corresponding electronic and polaronic effective masses in the available range of α (see Fig. 5 in ref. [27]). Outside of the available range we fit a smooth and continuous quartic function with a resulting best fit as follows:

$$\frac{m_{\text{P}}^*}{m^*} = \left(1.07\alpha^4 - 160.53\right)^{-1}.$$

(12)

The self-localization of the electron in the strong-coupling regime yields the notion of a "polaron radius", a_{P}. For instance, with a Gaussian ansatz for the electronic wavefunction, in the adiabatic limit one obtains:

$$\phi(\mathbf{r}) = \left(\frac{1}{a_{\text{P}}\sqrt{\pi}}\right)^{\frac{3}{2}} \exp\left(-\frac{\mathbf{r}^2}{2a_{\text{P}}^2}\right),$$

(13)

with

$$a_{\text{P}} = 3\sqrt{\frac{\pi}{2}} \frac{\epsilon^*}{m^*}.$$

(14)

Coherently, a_{P} is defined only in terms of quantities that do not depend on the nuclear masses. When a_{P} is on the order of the distance between equivalent atomic sites in the crystals, the Fröhlich model cannot be a good representation of the real material, as it is based on a continuum hypothesis for the vibrational degrees of freedom.

The generalized Fröhlich model

The standard Fröhlich model, valid under very restrictive hypotheses (isotropy, one phonon branch, one electronic band), can be generalized to include systems with degenerate and anisotropic band extrema, multiple phonon branches, and anisotropic dielectric functions[9]. Bands are still assumed to be parabolic in each direction and phonon energies are still constant with respect to the wavevector length q, but all might depend on its direction $\hat{\mathbf{q}}$. As in ref. [36], we treat both conduction and valence bands thanks to the integer variable σ, that is 1 for the conduction band (or electron polarons), and -1 for the valence band (or hole polarons). The Hamiltonian is then similar to that of Eq. (1),

$$\hat{H}^{\text{gFr}} = \sum_{\mathbf{k}n} \frac{\sigma\mathbf{k}^2}{2m_n^*(\hat{\mathbf{k}})} \hat{c}_{\mathbf{k}n}^{\dagger} \hat{c}_{\mathbf{k}n} + \sum_{\mathbf{q}j} \omega_{j0}(\hat{\mathbf{q}})\hat{a}_{\mathbf{q}j}^{\dagger} \hat{a}_{\mathbf{q}j} \\ + \sum_{\mathbf{q}j,\mathbf{k}n'n} g^{\text{gFr}}(\mathbf{q}j,\mathbf{k}n'n) \hat{c}_{\mathbf{k}+\mathbf{q}n'}^{\dagger} \hat{c}_{\mathbf{k}n} \left(\hat{a}_{\mathbf{q}j}^{\dagger} + \hat{a}_{-\mathbf{q}j}\right),$$

(15)

with $m_n^*(\hat{\mathbf{k}})$ the direction-dependent effective masses, $\mathbf{k}$ the electron wavevector, n the band index, $\omega_{j0}(\hat{\mathbf{q}})$ the direction-dependent phonon frequency, $\mathbf{q}$ the phonon wavevector and j the phonon branch index. The electron–phonon coupling constant is given by

$$g^{\text{gFr}}(\mathbf{q}j,\mathbf{k}n'n) = \frac{i}{q} \frac{4\pi}{\Omega_0} \left(\frac{1}{2\omega_{j0}(\mathbf{q})V_{\text{BvK}}}\right)^{1/2} \frac{\hat{\mathbf{q}} \cdot \mathbf{p}_j(\hat{\mathbf{q}})}{\epsilon^{\infty}(\hat{\mathbf{q}})} \\ \times \sum_m s_{n'm}(\hat{\mathbf{k}}')(s_{nm}(\hat{\mathbf{k}}))^*.$$

(16)

In these equations, the sum over n, n' and m runs only over the bands that connect to the degenerate extremum, that are renumbered from 1 to n_{deg}. The electron–phonon part also depends only on few quantities: the Born effective charges (entering the mode-polarity vectors $\mathbf{p}_j$ which are the Born charge weighted phonon displacement vectors), the macroscopic dielectric tensor ϵ^{∞}, and the phonon frequencies ω_{j0}, the primitive cell volume Ω_0, the Born-von Karman normalization volume V_{BvK} corresponding to the $\mathbf{k}$ and $\mathbf{q}$ samplings. The s_{nm} tensors are symmetry-dependent unitary matrices, similar to spherical harmonics. Finally, $\mathbf{k}' = \mathbf{k} + \mathbf{q}$.

In this generalized model, the ZPR for a band extremum can be obtained also at lowest order of perturbation theory, as

$$\text{ZPR}^{\text{gFr}} = -\sum_{jn} \frac{\sigma}{\sqrt{2}\Omega_0 n_{\text{deg}}} \int_{4\pi} d\hat{\mathbf{q}} \left(m_n^*(\hat{\mathbf{q}})\right)^{1/2} \times \left(\omega_{j0}(\hat{\mathbf{q}})\right)^{-3/2} \left(\frac{\hat{\mathbf{q}} \cdot \mathbf{p}_j(\hat{\mathbf{q}})}{\epsilon^{\infty}(\hat{\mathbf{q}})}\right)^2.$$

(17)

When comparing with the expression for the renormalization energy from the standard Fröhlich model, Eq. (9), we see that it is possible to re-write Eq. (17) in a similar way, highlighting the fact

that this expression originates from an average over $\hat{\mathbf{q}}$ directions, and summation over the contributions from different phonon branches;

$$\text{ZPR}^{\text{gFr}} = -\sigma \sum_j \left\langle a_j(\hat{\mathbf{q}}) \omega_{j0}(\hat{\mathbf{q}}) \right\rangle_{\hat{\mathbf{q}}}, \tag{18}$$

where

$$\left\langle f(\hat{\mathbf{q}}) \right\rangle_{\hat{\mathbf{q}}} = \frac{1}{4\pi} \int_{4\pi} d\hat{\mathbf{q}}\, f(\hat{\mathbf{q}}) \tag{19}$$

is an average over $\hat{\mathbf{q}}$ directions.

The $a_j(\hat{\mathbf{q}})$ parameters are defined by

$$a_j(\hat{\mathbf{q}}) = \frac{4\pi}{\sqrt{2}\Omega_0} \left(\frac{1}{n_{\text{deg}}} \sum_{n=1}^{n_{\text{deg}}} (m_n^*(\hat{\mathbf{q}}))^{1/2} \right) \times (\omega_{j0}(\hat{\mathbf{q}}))^{-1/2} \left(\frac{\hat{\mathbf{q}} \cdot \mathbf{p}_j(\hat{\mathbf{q}})}{\epsilon^\infty(\hat{\mathbf{q}}) \omega_{j0}(\hat{\mathbf{q}})} \right)^2, \tag{20}$$

and can also be re-written to look similar to Eq. (3),

$$a_j(\hat{\mathbf{q}}) = \frac{\left\langle (m_n^*(\hat{\mathbf{q}}))^{\frac{1}{2}} \right\rangle_n}{\epsilon_j^*(\hat{\mathbf{q}}) \sqrt{2\omega_{j0}(\hat{\mathbf{q}})}} \tag{21}$$

where

$$\frac{1}{\epsilon_j^*(\hat{\mathbf{q}})} = \frac{4\pi}{\Omega_0} \left(\frac{\hat{\mathbf{q}} \cdot \mathbf{p}_j(\hat{\mathbf{q}})}{\epsilon^\infty(\hat{\mathbf{q}}) \omega_{j0}(\hat{\mathbf{q}})} \right)^2 \tag{22}$$

replaces Eq. (4), while

$$\left\langle (m_n^*(\hat{\mathbf{q}}))^{\frac{1}{2}} \right\rangle_n = \frac{1}{n_{\text{deg}}} \sum_{n=1}^{n_{\text{deg}}} (m_n^*(\hat{\mathbf{q}}))^{1/2} \tag{23}$$

highlights that the effective mass entering Eq. (21) is an average over bands that are degenerate at the extremum. For a in the generalized Fröhlich model, we employ the expression

$$a^{\text{gFr}} = \sum_j \left\langle a_j(\hat{\mathbf{q}}) \right\rangle_{\hat{\mathbf{q}}}, \tag{24}$$

with $a_j(\hat{\mathbf{q}})$ given by Eq. (21).

To summarize, in the lowest order of perturbation theory treatment, the multiband, multibranch, anisotropic generalization of the simple Eq. (3) can be structured in the same way, with the band contribution being averaged, the branch contributions being summed, and the anisotropy being treated by an average over $\hat{\mathbf{q}}$ directions. The polaron formation energy writes

$$E_{\text{P}} = -\sum_j \left\langle \frac{\left\langle (m_n^*(\hat{\mathbf{q}}))^{\frac{1}{2}} \right\rangle_n}{\epsilon_j^*(\hat{\mathbf{q}})} \sqrt{\frac{\omega_{j0}(\hat{\mathbf{q}})}{2}} \right\rangle_{\hat{\mathbf{q}}}. \tag{25}$$

Note that σ does not appear in E_{P}.

A generalization of a to anisotropic, multibranch systems, $a_j(\hat{\mathbf{q}})$, had been tentatively defined by C. Verdi, see ref. [47], Eq. (4.12) page 62, however lacking both effective mass and phonon frequency dependencies on direction, and ignoring the possible electronic degeneracy.

From Eq. (25) one might examine the relevance of the following approximate decoupling between electronic and vibrational and dielectric contributions:

$$E_{\text{P}} \approx -\left\langle (m_n^*(\hat{\mathbf{q}}))^{\frac{1}{2}} \right\rangle_{\hat{\mathbf{q}}n} \left(\sum_j \left\langle \frac{1}{\epsilon_j^*(\hat{\mathbf{q}})} \sqrt{\frac{\omega_{j0}(\hat{\mathbf{q}})}{2}} \right\rangle_{\hat{\mathbf{q}}} \right). \tag{26}$$

The factorization of the $\left\langle (m_n^*(\hat{\mathbf{q}}))^{\frac{1}{2}} \right\rangle_{\hat{\mathbf{q}}n}$ term appears naturally and is exact in the cubic case, as shown below.

The generalized Fröhlich model in cubic systems

For a cubic system, even with several phonon branches, there is no dependence on the direction of $\mathbf{q}$ for the phonon frequencies

and dielectric properties. The Hamiltonian becomes [36,46]

$$\hat{H}^{\text{cFr}} = \sum_{\mathbf{k}n} \frac{\sigma \mathbf{k}^2}{2m_n^*(\mathbf{k})} \hat{c}_{\mathbf{k}n}^\dagger \hat{c}_{\mathbf{k}n} + \sum_{\mathbf{q}j} \omega_{j\text{LO}} \hat{a}_{\mathbf{q}j}^\dagger \hat{a}_{\mathbf{q}j}$$
$$+ \sum_{\mathbf{k}n'n, \mathbf{q}j} g^{\text{cFr}}(\mathbf{q}j, \mathbf{k}n'n) \hat{c}_{\mathbf{k}+\mathbf{q}n'}^\dagger \hat{c}_{\mathbf{k}n} \left(\hat{a}_{\mathbf{q}j}^\dagger + \hat{a}_{-\mathbf{q}j} \right), \tag{27}$$

with a slightly simplified electron–phonon coupling constant given by

$$g^{\text{cFr}}(\mathbf{q}j, \mathbf{k}n'n) = \frac{14\pi}{q\Omega_0} \left(\frac{1}{2\omega_{j\text{LO}} V_{\text{BvK}}} \right)^{1/2} \frac{p_{j\text{LO}}}{\epsilon^\infty}$$
$$\times \sum_m s_{n'm}(\hat{\mathbf{k}}')(s_{nm}(\hat{\mathbf{k}}))^*. \tag{28}$$

The suppression of the "i" prefactor from Eq. (16) to Eq. (28) is related to the Born and Huang convention [46]. Still working in the lowest order of perturbation theory, Eq. (18) can be re-written as a linear combination of a_j parameters and phonon frequencies at Γ,

$$\text{ZPR}^{\text{cFr}} = -\sigma \sum_j a_j \omega_{j\text{LO}}, \tag{29}$$

with each a_j being

$$a_j = \frac{\left\langle (m_n^*(\hat{\mathbf{q}}))^{\frac{1}{2}} \right\rangle_{\hat{\mathbf{q}}n}}{\epsilon_j^* \sqrt{2\omega_{j\text{LO}}}} \tag{30}$$

The numerator is purely electronic, and independent of the j index, while the denominator is purely dielectric and dynamical. This simplification appears only for the cubic crystallographic system. A similar decoupling appears for the polaron energy:

$$E_{\text{P}} = -\left\langle (m_n^*(\hat{\mathbf{q}}))^{\frac{1}{2}} \right\rangle_{\hat{\mathbf{q}}n} \left(\sum_j \frac{\sqrt{\omega_{j\text{LO}}}}{\epsilon_j^* \sqrt{2}} \right). \tag{31}$$

These equations shed light on the relationship between the standard and generalized Fröhlich model. They will provide guidance for the choice of the parameters for the standard Fröhlich model, which follows below.

Parameterization of the standard Frohlich model

Because of its simplicity, and since a vast amount of results have been gathered for the standard Fröhlich model, the treatment of real materials using this model is very desirable, even in cases where its basic hypotheses do not apply. The standard Fröhlich model relies on the ω_{LO} frequency, the m^* effective mass and the ionic part of the (isotropic) dielectric tensor, ϵ^*, actually a scalar. They combine to deliver the a parameter, and to predict a polaron formation energy E_{P} (or ZPR) obtained in the full range of values from diagrammatic Monte Carlo or Feynman path integral approaches [26,27].

In order to define a standard Fröhlich model for any given material, we must extract a single effective electronic mass m_{sFr}^*, an effective dielectric constant ϵ_{sFr}^*, and a single effective LO phonon frequency, $\omega_{\text{eff}}^{\text{sFr}}$. Such oversimplification applies exactly only to a few materials, namely binary (and some ternary cubic) materials with the electron or hole pockets situated at Γ. In this section, we define such parameters for general systems, inspired by the simplifications happening for cubic material above, and also from previously existing averaging procedures from the literature.

As concerns the electronic effective mass, for the standard Fröhlich model, we will use the directional average of effective masses,

$$m_{\text{sFr}}^* = \left(\left\langle (m_n^*(\hat{\mathbf{q}}))^{\frac{1}{2}} \right\rangle_{\hat{\mathbf{q}}n} \right)^2, \tag{32}$$

where, coherently with Eqs. (19) and (23)

$$\left\langle (m_n^*(\hat{\mathbf{q}}))^{\frac{1}{2}} \right\rangle_{\hat{\mathbf{q}}n} = \frac{1}{4\pi} \int_{4\pi} d\hat{\mathbf{q}} \frac{1}{n_{\mathrm{deg}}} \sum_{n=1}^{n_{\mathrm{deg}}} (m_n^*(\hat{\mathbf{q}}))^{1/2}. \tag{33}$$

For cubic systems, this expression accounts exactly for the anisotropy in the effective masses and for the possible degeneracies, as discussed in Sec. III C. For non-cubic systems, there is no such decoupling of the effective mass factor from the dielectric and dynamical ones, as Eq. (26) is not exact.

The anisotropy of the dielectric constants (ϵ^∞, ϵ^0, and ϵ^*) is suppressed by the generic definition

$$1/\epsilon_{\mathrm{sFr}} = \mathrm{Tr}(\epsilon^{-1})/3. \tag{34}$$

For the effective LO frequency, both the multibranch character and the directional dependence must be suppressed. It might be possible to use the largest LO frequency. Of course this is exact for cubic binary materials, for which there is only one LO frequency. In moderately complex cubic materials, it is also expected that the largest LO frequency should be the one with the biggest effective IR activity, hence dominating the electron–phonon coupling behavior. But one can imagine systems for which an average over different LO frequencies should be made. In isotropic case, Hellwarth and Biaggio[42] have proposed a way to average over all LO modes, considered in the context of Feynman's variational path integral approach[26].

We focus first on the isotropic situation. Hellwarth and Biaggio[42] proposes two approaches to define an effective LO phonon frequency in the isotropic multiphonon case. We follow a similar line of thought, although slightly simplified (i.e. it corresponds to the high-temperature regime of the first approach), and with an additional approximation. Then, a plausible generalization to the anisotropic Born effective charge case is proposed, still based on isotropic dielectric tensors. This generalization is used in the main text.

Following ref. [42], one first introduces W_i, the coupling between the LO phonon number i and a single electron in the conduction band. The square of the effective coupling between the effective LO phonon mode and that electron, W_e^2, is obtained by summing the square of the specific couplings,

$$W_e^2 = \sum_{i=1}^m W_i^2. \tag{35}$$

The square of the effective LO frequency is obtained as the harmonic average of the square of the phonon frequencies, weighted by the ratio between the square of each coupling and the sum of the squares of the couplings,

$$\frac{1}{\Omega_e^2} = \sum_{i=1}^m \left(\frac{W_i^2}{W_e^2} \right) \frac{1}{\Omega_i^2}. \tag{36}$$

Being the sum of positive quantities multiplied by positive weights summing to one, the effective phonon frequency must be between the minimal and the maximal LO phonon frequencies.

Hellwarth and Biaggio[42] also shows how to treat the dielectric response of the material, in the infra-red range, by the adiabatic approximation, giving

$$\frac{1}{\epsilon^\infty} - \frac{1}{\epsilon(\omega)} = \sum_{i=1}^m \frac{W_i^2}{\Omega_i^2 - \omega^2}. \tag{37}$$

The low-frequency limit yields the effective dielectric function as in Eq. (37) of ref. [42],

$$\frac{1}{\epsilon^*} = \frac{1}{\epsilon^\infty} - \frac{1}{\epsilon(\omega=0)} = \sum_{i=1}^m \frac{W_i^2}{\Omega_i^2} = \frac{W_e^2}{\Omega_e^2}. \tag{38}$$

The ratio between the two effective quantities is thus fixed by the knowledge of ϵ^*.

The determination of W_e^2 can be obtained by considering Eq. (37) for large values of ω (albeit lower than the electronic excitations). We get

$$W_e^2 = \sum_{i=1}^m W_i^2 = \lim_{\substack{\omega \text{ large} \\ \omega < E_{\mathrm{gap}}}} \left[\omega^2 \left(\frac{1}{\epsilon(\omega)} - \frac{1}{\epsilon^\infty} \right) \right]. \tag{39}$$

The dielectric function can alternatively be formulated in terms of LO and TO frequencies and the different dielectric quantities. Indeed, the difference of inverse of dielectric responses present in Eqs, (37)–(39) can be re-written thanks to Eq. (64) of ref. [48],

$$\frac{1}{\epsilon(\omega)} - \frac{1}{\epsilon^\infty} = \frac{1}{\epsilon^\infty} \left(\prod_{i=1}^m \left(\frac{\omega_i^2(\mathbf{q}=\mathbf{0}) - \omega^2}{\omega_i^2(\mathbf{q}\to\mathbf{0}) - \omega^2} \right) - 1 \right), \tag{40}$$

where $\omega_i(\mathbf{q}=\mathbf{0})$ are TO phonon frequencies, and $\omega_i(\mathbf{q}\to\mathbf{0}) = \Omega_i$ are LO frequencies. Then, the limit of Eq. (40) multiplied by ω^2 is taken for large ω,

$$\lim_{\substack{\omega \text{ large} \\ \omega < E_{\mathrm{gap}}}} \left[\omega^2 \left(\frac{1}{\epsilon(\omega)} - \frac{1}{\epsilon^\infty} \right) \right] = \frac{1}{\epsilon^\infty} \sum_{i=1}^m (\omega_i^2(\mathbf{q}\to\mathbf{0}) - \omega_i^2(\mathbf{q}=\mathbf{0})).$$

$$\tag{41}$$

This equation is inserted back into Eq. (39), then Eq. (38) is used to determine the effective frequency in terms of difference of squares of LO and TO phonon frequencies, with dielectric rescaling.

$$\Omega_e^2 = \left(\frac{\epsilon^*}{\epsilon^\infty} \right) \sum_{i=1}^m (\omega_i^2(\mathbf{q}\to\mathbf{0}) - \omega_i^2(\mathbf{q}=\mathbf{0})). \tag{42}$$

This result is obtained without approximation, in the case of an isotropic multiphonon system.

Furthermore, in case we neglect mode mixing (so, supposing that LO and TO modes have the same eigenvectors), we can connect the effective frequency to the macroscopic parameters of our system and to the isotropic Born effective charges Z_κ of nucleus κ, using Eq. (63) of ref. [48], namely,

$$\Omega_e^2 = \frac{\epsilon^*}{(\epsilon^\infty)^2} \frac{4\pi}{\Omega_0} \sum_\kappa \frac{Z_\kappa^2}{M_\kappa} \tag{43}$$

where Ω_0 is the primitive cell volume, and M_κ the mass of the nucleus κ.

We finally generalize this formula to the anisotropic Born effective charge case, to obtain our effective LO phonon frequency $\omega_{\mathrm{eff}}^{\mathrm{sFr}}$,

$$(\omega_{\mathrm{eff}}^{\mathrm{sFr}})^2 = \frac{\epsilon^*}{(\epsilon^\infty)^2} \frac{4\pi}{\Omega_0} \sum_{\kappa\alpha\beta} \frac{\left(Z_{\kappa,\alpha\beta}^* \right)^2}{3M_\kappa} \tag{44}$$

where α and β runs over the three cartesian directions. This formula might seem strange, as it does not take the form of an average over LO modes. However, simplifying for the case of isotropic dielectric behavior we obtain

$$(\omega_{\mathrm{eff}}^{\mathrm{sFr}})^2 = \frac{\epsilon_{\mathrm{sFr}}^*}{(\epsilon^\infty)^2} \frac{4\pi}{\Omega_0} \sum_k \frac{(Z_k^*)^2}{M_k}, \tag{45}$$

Like for the isotropic case, it is expected that $\omega_{\mathrm{eff}}^{\mathrm{sFr}}$ never exceeds the biggest LO phonon frequency along all possible directions, and also that $\omega_{\mathrm{eff}}^{\mathrm{sFr}}$ is never lower than the smallest LO phonon frequency along all possible directions, although we have not tried to prove this assertion.

Noteworthy, the use of an effective LO frequency provides coherence in treating systems more complex than binary ones

when a global dielectric constant is used in expressing polaron properties. Therefore, in the standard Fröhlich model, the ZPR and coupling constant α are considered as follows from now on:

$$E_P \approx -\alpha^{sFr}\omega_{eff}^{sFr}, \tag{46}$$

and

$$\alpha^{sFr} = \frac{1}{\epsilon_{sFr}^*}\sqrt{\frac{m_{sFr}^*}{2\omega_{eff}^{sFr}}}. \tag{47}$$

An automatic python workflow has been created to obtain the electronic effective masses and store them in a database. The input files for ABINIT[49,50] were generated using AbiPy[49,50] by inserting the ground-state parameters from the Materials Project database. The valence band maximum (VBM) and conduction band minimum (CBM) were then determined by AbiPy by producing the electronic band structure along the high-symmetry paths of each system's Brillouin zone. The effective mass tensors at these points were determined by calculating the second-order derivative of the VBM and CBM eigenenergies with respect to the wavevector $\mathbf{k}$, including the effect of band degeneracies and warping[44], within Density Functional Perturbation Theory (DFPT)[51], as implemented in ABINIT.

Non-adiabatic Allen-Heine-Cardona methods

From the high-throughput calculations within the Fröhlich model we focus on a few materials calculated within the non-adiabatic Allen-Heine-Cardona (AHC)[16,17] theory. Comparing the two approaches, the former only includes long-wavelength fields of longitudinal optical phonons, while excluding short-range fields, non-LO vibration modes, second-order coupling to the atomic displacements, also known as the Debye-Waller (DW) self-energy, inter-band contributions, and non-parabolic effective masses which are included in the latter.

The electronic and phonon properties were calculated using ABINIT. To quantify the interaction between phonons and electrons we apply the lowest order of many-body perturbation theory which is sufficient[52] to describe the electron–phonon interactions in the quasi-particle self-energy. The self-energy contains two terms: the static Debye-Waller (DW)[53], and the dynamic Fan (FAN)[54] terms,

$$\Sigma_{\mathbf{k}n}(\omega) = \Sigma_{\mathbf{k}n}^{DW} + \Sigma_{\mathbf{k}n}^{FAN}(\omega). \tag{48}$$

The non-adiabatic AHC ZPR is obtained directly from the real part of the self-energy evaluated at the Kohn-Sham (KS) using Density Functional Theory (DFT) electronic energy $\varepsilon_{\mathbf{k}n}$ in a state defined by the wave-vector $\mathbf{k}$ and the band n,

$$ZPR_{\mathbf{k}n} = \Re e\Sigma(\omega = \varepsilon_{\mathbf{k}n}). \tag{49}$$

The non-adiabatic method includes the contribution of the phonons frequencies to the Fan denominator, representing the retarded movement of the electrons forced by the ionic motion, and at 0 K temperature it can be described as

$$\Sigma_{\mathbf{k}n}^{Fan}(\omega) = \frac{1}{N_q}\sum_{\mathbf{q}}^{BZ}\sum_{j}\sum_{n'}\left|\left\langle \mathbf{k}+\mathbf{q}n'\left|H_{\mathbf{q}j}^{(1)}\right|\mathbf{k}n\right\rangle\right|^2$$
$$\times\left[\frac{1-f_{\mathbf{k}+\mathbf{q}n'}}{\omega-\varepsilon_{\mathbf{k}+\mathbf{q}n'}-\omega_{\mathbf{q}j}+i\eta}+\frac{f_{\mathbf{k}+\mathbf{q}n'}}{\omega-\varepsilon_{\mathbf{k}+\mathbf{q}n'}+\omega_{\mathbf{q}j}+i\eta}\right]. \tag{50}$$

The phonon's contributions to the self-energy are included in the sum of the phonon frequencies, $\omega_{\mathbf{q}j}$, over the phonon wavevectors $\mathbf{q}$ in the Brillouin Zone and the phonon modes j. There is also the contribution of the scattering of electron from state $|\mathbf{k}n\rangle$ to the state $|\mathbf{k}+\mathbf{q}n'\rangle$ due to the perturbation $H^{(1)}$ of the $\mathbf{q}j$ phonon. These terms are determined within Density Functional Perturbation Theory (DFPT). The scattered potentials in $H^{(1)}$ is first calculated in a coarse q-mesh grid and then interpolated to a finer q-mesh. In this Fourier-based interpolation, we removed the

dipole term before the interpolation to treat the non-analytical behavior at long wave-length and added them after, more details can be found in refs. [39,40].

In Section IV, we will split $\Sigma_{\mathbf{k}n}^{Fan}$ into its wave-vector $\mathbf{q}$ or phonon mode j components and remove the sum in Eq. (50) of the correspondent component. The self-energy becomes $\Sigma_{\mathbf{q}\mathbf{k}n}^{Fan}$ or $\Sigma_{j\mathbf{k}n}^{Fan}$, respectively. Separating the FAN self-energy by each phonon mode allow us to verify which mode contributes the most to the ZPR. In addition, introducing the phonon frequencies at Γ, except the acoustic modes, we can compare the coupling strength for each mode as it is done in the generalized Fröhlich model,

$$ZPR_{\mathbf{k}n} = \sum_{j}a_j\omega_{j0} \tag{51}$$

where $a_j = ZPR_{j\mathbf{k}n}/\omega_{j0}$.

The DW self-energy is determined using the acoustic sum rule within the rigid-ion approximation[16], and its formulation is detailed in ref. [7].

DATA AVAILABILITY

CODE AVAILABILITY

REFERENCES

1. Cardona, M. & Thewalt, M. Isotope effects on the optical spectra of semiconductors. *Rev. Mod. Phys.* **77**, 1173–1224 (2005).
2. Shishkin, M., Marsman, M. & Kresse, G. Accurate quasiparticle spectra from self-consistent GW calculations with vertex corrections. *Phys. Rev. Lett.* **99**, 246403 (2007).
3. Marini, A. Ab-initio finite temperature excitons. *Phys. Rev. Lett.* **101**, 106405 (2008).
4. Giustino, F., Louie, S. & Cohen, M. Electron-phonon renormalization of the direct band gap of diamond. *Phys. Rev. Lett.* **105**, 265501 (2010).
5. Moser, S. et al. Tunable polaronic conduction in anatase TiO₂. *Phys. Rev. Lett.* **110**, 196403 (2013).
6. Antonius, G., Poncé, S., Boulanger, P., Côté, M. & Gonze, X. Many-body effects on the zero-point renormalization of the band structure. *Phys. Rev. Lett.* **112**, 215501 (2014).
7. Poncé, S. et al. Temperature dependence of the electronic structure of semiconductors and insulators. *J. Chem. Phys.* **143**, 102813 (2015).
8. Verdi, C., Caruso, F. & Giustino, F. Origin of the crossover from polarons to Fermi liquids in transition metal oxides. *Nat. Commun.* **8**, 15769 (2017).
9. Miglio, A. et al. Predominance of non-adiabatic effects in zero-point renormalization of the electronic band gap. *Npj Comput. Mater.* **6**, 167 (2020).
10. Hohenberg, P. & Kohn, W. Inhomogeneous electron gas. *Phys. Rev.* **136**, B864–B871 (1964).
11. Kohn, W. & Sham, L. J. Self-consistent equations including exchange and correlation effects. *Phys. Rev.* **140**, A1133–A1138 (1965).
12. Martin, R. M. *Electronic structure. Theory and practical methods.* (Cambridge University Press, Cambridge, United Kingdom, 2004).
13. Hedin, L. New method for calculating the one-particle green's function with application to the electron-gas problem. *Phys. Rev. B* **139**, A 796 (1965).
14. Martin, R. M., Reining, L. & Ceperley, D. M. *Interacting Electrons. Theory and Computational Approaches* (Cambridge University Press, Cambridge, United Kingdom, 2016).
15. Fröhlich, H. Interaction of electrons with lattice vibrations. *Proc. R. Soc. A: Math* **215**, 291–298 (1952).
16. Allen, P. B. & Heine, V. Theory of the temperature dependence of electronic band structures. *J. Phys. C* **9**, 2305–2312 (1976).

17. Allen, P. B. & Cardona, M. Theory of the temperature dependence of the direct gap of germanium. *Phys. Rev. B* **23**, 1495–1505 (1981).

18. Allen, P. & Cardona, M. Temperature dependence of the direct gap of Si and Ge. *Phys. Rev. B* **27**, 4760 (1983).

19. Verdi, C. & Giustino, F. Fröhlich electron-phonon vertex from first principles. *Phys. Rev. Lett.* **115**, 176401 (2015).

20. Giustino, F. Electron-phonon interactions from first principles. *Rev. Mod. Phys.* **89**, 015003 (2017).

21. Sio, W. H., Verdi, C., Poncé, S. & Giustino, F. Polarons from first principles, without supercells. *Phys. Rev. Lett.* **122**, 246403 (2019).

22. Brown-Altvater, F. et al. Band gap renormalization, carrier mobilities, and the electron-phonon self-energy in crystalline naphthalene. *Phys. Rev. B* **101**, 165102 (2020).

23. Brousseau-Couture, V., Godbout, E., Côté, M. & Gonze, X. Zero-point lattice expansion and band gap renormalization: Grüneisen approach versus free energy minimization. *Phys. Rev. B* **106**, 085137 (2022).

24. Brousseau-Couture, V., Godbout, E., Côté, M. & Gonze, X. Effect of spin-orbit coupling on the zero-point renormalization of the electronic band gap in cubic materials: first principles calculations and generalized fröhlich model. *Phys. Rev. B* **107**, 115173 (2023).

25. Devreese, J. T. Fröhlich polarons from 0D to 3D: concepts and recent developments. *J. Condens. Matter Phys.* **19**, 255201 (2007).

26. Feynman, R. P. Slow electrons in a polar crystal. *Phys. Rev.* **97**, 660–665 (1955).

27. Mishchenko, A., Prokof'ev, N., Sakamoto, A. & Svistunov, B. Diagrammatic quantum Monte Carlo study of the Fröhlich polaron. *Phys. Rev. B* **62**, 6317–6336 (2000).

28. Vasilchenko, V., Zhugayevych, A. & Gonze, X. Variational Polaron Equations Applied to the Anisotropic Fröhlich Model. *Phys. Rev. B* **105**, 214301 (2022).

29. Lafuente-Bartolome, J. et al. Unified approach to polarons and phonon-induced band structure renormalization. *Phys. Rev. Lett.* **129** (2022).

30. Lafuente-Bartolome, J. et al. Ab initio self-consistent many-body theory of polarons at all couplings. *Phys. Rev. B* **106**, 075119 (2022).

31. Franchini, C., Reticcioli, M., Setvin, M. & Diebold, U. Polarons in materials. *Nat. Rev. Mater.* **6**, 560 (2021).

32. Holstein, T. Studies of polaron motion: Part I. the molecular-crystal model. *Ann. Phys.* **8**, 325–342 (1959).

33. Holstein, T. Studies of polaron motion: Part II. The "small" polaron. *Ann. Phys.* **8**, 343–389 (1959).

34. Petretto, G. et al. High-throughput density-functional perturbation theory phonons for inorganic materials. *Sci. Data* **5**, 180065 (2018).

35. Hautier, G., Miglio, A., Waroquiers, D., Rignanese, G.-M. & Gonze, X. How Does Chemistry Influence Electron Effective Mass in Oxides? A High-Throughput Computational Analysis. *Chem. Mater.* **26**, 5447 (2014).

36. Guster, B. et al. Fröhlich polaron effective mass and localization length in cubic materials: Degenerate and anisotropic electronic bands. *Phys. Rev. B* **104**, 235123 (2021).

37. Gordy, W. New Method of Determining Electronegativity from Other Atomic Properties. *Phys. Rev.* **69**, 604 (1946).

38. Nery, J. P. et al. Quasiparticles and phonon satellites in spectral functions of semiconductors and insulators: Cumulants applied to the full first-principles theory and the fröhlich polaron. *Phys. Rev. B* **97**, 115145 (2018).

39. Brunin, G. et al. Phonon-limited electron mobility in Si, GaAs and GaP with exact treatment of dynamical quadrupoles. *Phys. Rev. B* **102**, 094308 (2020).

40. Brunin, G. et al. Electron-phonon beyond Fröhlich: dynamical quadrupoles in polar and covalent solids. *Phys. Rev. Lett.* **125**, 136601 (2020).

41. Abreu, J. C., Nery, J. P., Giantomassi, M., Gonze, X. & Verstraete, M. J. Spectroscopic signatures of nonpolarons : the case of diamond. *Phys. Chem. Chem. Phys.* **24**, 12580–12591 (2022).

42. Hellwarth, R. W. & Biaggio, I. Mobility of an electron in a multimode polar lattice. *Phys. Rev. B* **60**, 299–307 (1999).

43. Fröhlich, H. Electrons in lattice fields. *Adv. Phys.* **3**, 325–361 (1954).

44. Mecholsky, A. N., Resca, L., Pegg, I. L. & Fornari, M. Theory of band warping and its effects on thermoelectronic transport properties. *Phys. Rev. B* **89**, 155134 (2014).

45. Mahan, G. D. *Many-Particle Physics*. Physics of solids and liquids (Kluwer Academic, 2000), 3rd edn.

46. Guster, B. et al. Erratum : Fröhlich polaron effective mass and localization length in cubic materials: Degenerate and anisotropic electronic bands. *Phys. Rev. B* **105**, 119902 (2022).

47. Verdi, C. *First-principles Fröhlich electron-phonon coupling and polarons in oxides and polar semiconductors*. PhD thesis, U. of Oxford, Oxford, UK (2017).

48. Gonze, X. & Lee, C. Dynamical matrices, born effective charges, dielectric permittivity tensors, and interatomic force constants from density-functional perturbation theory. *Phys. Rev. B* **55**, 10355–10368 (1997).

49. Gonze, X. et al. The Abinit project: Impact, environment and recent developments. *Comput. Phys. Commun.* **248**, 107042 (2020).

50. Romero, A. H. et al. ABINIT: Overview, and focus on selected capabilities. *J. Chem. Phys.* **152**, 124102 (2020).

51. Janssen, J. L. et al. Precise effective masses from density functional perturbation theory. *Phys. Rev. B* **93**, 205147 (2016).

52. Migdal, A. B. Interaction between electrons and lattice vibrations in a normal metal. *Zh. Eksp. Teor. Fiz.* **34**, 1438 (1958).

53. Antoncik, E. On the theory of temperature shift of the absorption curve in non-polar crystals. *Czechoslovak Journal of Physics* **5**, 449 (1955).

54. Fan, H. Y. Temperature dependence of the energy gap in semiconductors. *Phys. Rev.* **82**, 900–905 (1951).

AUTHOR CONTRIBUTIONS

P.M.M.C.M. and J.C.A. both wrote the subroutines and performed the high-throughput calculations for the results of the standard and generalized Fröhlich models. J.C.A. performed the calculations using the AHC model. B.G. performed the statistical analysis and the computation of the standard ZPR using Feynman's path integral expressions. X.G. derived the effective LO phonon frequency for the standard Frohlich model. M.V. and X.G. conceived the project. All authors discussed frequently the project, gave suggestions, and were involved in the writing and reviewing of the manuscript.

COMPETING INTERESTS

The authors declare no competing interests.

ADDITIONAL INFORMATION

Supplementary information The online version contains supplementary material available at https://doi.org/10.1038/s41524-023-01083-8.

Correspondence and requests for materials should be addressed to Pedro Miguel M. C. de Melo.

Reprints and permission information is available at http://www.nature.com/reprints

Publisher's note Springer Nature remains neutral with regard to jurisdictional claims in published maps and institutional affiliations.